Received: 8 November 2021 | Accepted: 24 June 2022

DOI: 10.1111/bpa.13109

RESEARCH ARTICLE

Brain Pathology

Attenuation of Piwil2 induced by hypoxic postconditioning prevents cerebral ischemic injury by inhibiting *CREB2* promoter methylation

Lixuan Zhan[1] | **Meiyan Chen**[1] | **Taoyan Pang**[1] | **Xinyu Li**[1] | **Long Long**[1] | **Donghai Liang**[2] | **Linhui Peng**[1] | **Weiwen Sun**[1] | **En Xu**[1]

[1]Institute of Neurosciences and Department of Neurology of the Second Affiliated Hospital of Guangzhou Medical University and Key Laboratory of Neurogenetics and Channelopathies of Guangdong Province and the Ministry of Education of China, Guangzhou, China

[2]Department of Environmental Health Sciences, Rollins School of Public Health, Emory University, Atlanta, Georgia, USA

Correspondence
En Xu, Institute of Neurosciences and Department of Neurology of the Second Affiliated Hospital of Guangzhou Medical University, 250 Changgang Dong RD, Guangzhou 510260, China.
Email: enxu@163.net

Funding information
National Natural Science Foundation of China, Grant/Award Numbers: 81873745, 81971124; Science and Technology Program of Guangzhou, China, Grant/Award Number: 202002030072

Abstract

Epigenetic modification contributes to the pathogenesis of cerebral ischemia. Piwil2 belongs to the PIWI proteins subfamily and has a key role in the regulation of gene transcription through epigenetics. However, the roles of Piwil2 in cerebral ischemia have not been investigated. In this study, we aim to elucidate the roles and the underlying molecular mechanisms of Piwil2 in ischemic tolerance induced by hypoxic postconditioning (HPC) against transient global cerebral ischemia (tGCI). We found that the expression of Piwil2 in CA1 was downregulated by HPC after tGCI. Silencing Piwil2 with antisense oligodeoxynucleotide (AS-ODN) in CA1 after tGCI decreased the expression of apoptosis-related proteins and exerted neuroprotective effects. Opposite results were observed after overexpression of Piwil2 induced by administration of Piwil2-carried lentivirus. Furthermore, we revealed differentially expressed Piwil2-interacting piRNAs in CA1 between HPC and tGCI groups by RNA binding protein immunoprecipitation (RIP) assay. Moreover, downregulating Piwil2 induced by HPC or AS-ODN after tGCI caused a marked reduction of DNA methyltransferase 3A (DNMT3A), which in turn abolished the tGCI-induced increase in the DNA methylation of *cyclic AMP response element-binding 2* (*CREB2*), thus increasing mRNA and protein of CREB2. Finally, downregulating Piwil2 restored dendritic complexity and length, prevented the loss of dentritic spines, thereby improving cognitive function after tGCI. These data firstly reveal that Piwil2 plays an important part in HPC-mediated neuroprotection against cerebral ischemia through epigenetic regulation of CREB2.

KEYWORDS
cerebral ischemia, CREB2, DNA methylation, hypoxic postconditioning, Piwil2

1 | INTRODUCTION

Stroke is the second leading cause of mortality and a major cause of long-term disability worldwide [1, 2], with ischemic stroke accounting for at least 80% of all strokes. It is well known that the pathogenesis of ischemic stroke is complicated, with various genetic and environmental factors involved. Accumulating evidence suggests that epigenetic alterations including DNA methylation, mRNA silencing and histone modification is involved in

Lixuan Zhan and Meiyan Chen contributed equally to this work.

the development of cerebral ischemia [3–5]. More specifically, current studies have indicated that changes in DNA methylation status play an important role in ischemic stroke [5–7]. Thus, epigenetics may provide diagnostic and therapeutic targets for ischemic stroke.

The P-element induced wimpy testis (PIWI) pathway, comprised of Piwi-interacting RNAs (piRNAs) and Piwi-like proteins, is involved in maintaining genome stability through RNA interference or epigenetic modification of gene expression. PiRNAs are a novel class of small non-coding RNAs, while Piwi-like proteins, belonging to the Argonaute family, are associated with piRNAs, and they take part in the biogenesis, transport, and the use of piRNAs [8]. Although it has long been thought that the expression and function of piRNAs and Piwi-like proteins are restricted to the germline, increasing lines of evidence indicate that they are related to the cell survival during certain physiological and pathological events [9]. Specifically, the PIWI pathway is functional in neuronal gene regulation in invertebrate and rodents neurons [10–14]. Until now, four members of the Piwi-like proteins, namely, Piwi-like RNA-mediated gene silencing (Piwil) 1/Hiwi, Piwil2/Hili, Piwil3, and Piwil4/Hiwi2, have been identified in the human genome. Similarly, three distinct Piwi proteins are detectable in rodents such as mouse and rat (Piwil1/Miwi, Piwil2/Mili, and Piwil4/Miwi2) [15]. Among them, Piwil2 is widely expressed in various types of tumors and inhibits apoptosis in tumor cells [16, 17]. In particular, low-level expression of truncated Piwil2 was identified in the adult mouse brain, and the knockout of *Piwil2* resulted in hypomethylation of transposons and behavioral defects [18]. It is intriguing to investigate whether Piwil2 can be expressed and has functional roles through interaction with epigenetic factors in the rat brain after cerebral ischemia.

Piwi-like proteins can exert its epigenetic function through DNA methylation. Generally, DNA methylation occurs on CpG islands and its step is carried out by DNA methyltransferases (DNMTs). In fetal Piwil2 and Piwil4-null testes of mice, the CpG methylation level in primordial germ cells is reduced, with concordant transposon upregulation [19–21]. Strikingly, PIWI pathway is shown to direct DNA methylation on a non-transposon locus to regulate gene expression. For instance, Rajasethupathy et al [10] demonstrated that the PIWI pathway enhanced long-term learning-related synaptic plasticity in *Aplysia* neurons by DNA methylation on non-transposon genomic regions, cyclic AMP response element-binding 2 (CREB2) promoter. CREB2 also acted as the activating transcription factor 4 (ATF4), which has been shown to be crucial to many physiological and pathological conditions [22]. There was a study revealing the involvement of CREB2 in endoplasmic reticulum stress [23], hypoxic resistance [24], and cerebral ischemia [25, 26]. CREB2 has been reported as a crucial modulator of neuronal plasticity and memory [27, 28]. The possible mechanisms of modulating CREB2-mediated transcription include post-translational control and epigenetic modifications [29]. CREB2 is extensively regulated at the post-translational level. Some modifications, such as phosphorylation, ubiquitination and acetylation, are perceived to affect CREB2 stability or transcriptional activity [29], whereas the function of epigenetic modifications remains obscure. Furthermore, given the fact that the DNA binding specificity of CREB2 can be altered by the methylation of DNA motifs [30], it is plausible that Piwil2 might exert its epigenetic functions by modulating the DNA methylations within CpG island of *CREB2* promoters, thereby contributing to the neuronal damage after cerebral ischemia.

The CA1 pyramidal neurons in hippocampus, an area crucial for learning and memory, have been shown to be subject to selective and delayed cell death after transient global cerebral ischemia (tGCI) [31]. Also, dendritic spines are deemed the structures essential to the learning and memory [32]. As one of the most energy-consuming structures of neurons, dendrites and their spines represent the most vulnerable structure after cerebral ischemia [33, 34]. Fortunately, it is generally believed that the damaged dendrites and spines could be restored if the pathological insults were relieved in a timely manner, or if the therapeutic interventions were applied in time. We previously reported that hypoxic postconditioning (HPC) ameliorated CA1 neuronal death induced by tGCI in rats [35]. However, it is still unclear whether HPC can enhance the plasticity of dendritic spines of pyramidal neurons in CA1 and improve memory function after tGCI. Moreover, the mechanism for reversible restoration of dendritic spines after ischemic stroke remains partially understood. Intriguingly, one PIWI/piRNA complex was shown to modulate dendritic spine development in the mouse hippocampus [36]. In addition, downregulation of CREB2 in rodent hippocampal neurons reduced the density of dendritic mushroom spines in vitro and in vivo [27, 28], and impaired synaptic plasticity [28]. Therefore, we hypothesize that HPC can downregulate Piwil2/piRNAs complex, thereby increasing the expression of CREB2 by inhibiting DNA methylation of *CREB2* induced by DNMT3A, and leading to the enhancement of neuroplasticity and neuroprotection after tGCI.

In the present study, we aimed to investigate how Piwil2 regulate the expression of CREB2 through DNA methylation in CA1 of rats after tGCI with HPC. Specifically, we demonstrate that HPC decreases the expression of Piwil2, leads to an increase in CREB2 by inhibiting *CREB2* promoter methylation mediated by DNMT3A, and ultimately causes an enhancement of neuroplasticity and neuroprotection after tGCI. This is the first report regarding a novel role of Piwil2 through epigenetic regulation of CREB2 in neuroprotection provided by HPC against tGCI in rats.

2 | MATERIALS AND METHODS

2.1 | Animals

Experiments were performed on adult male Wistar rats weighing 220–280 g (7–8 weeks old; Southern Medical University, Guangzhou, China). All surgical operations and animal experiments were conducted according to the *Animal Research: Reporting In Vivo Experiments (ARRIVE)* guidelines and were monitored by the Animals Care and Use Committee of Guangzhou Medical University (Guangzhou, China). Rats were housed in a temperature-controlled (22°C ± 1°C) and 12-h light/dark cycle environment with ad libitum access to food and water. Every effort had been made to minimize the number of animals used and to reduce animal suffering and distress.

2.2 | Transient global cerebral ischemia and hypoxic postconditioning

As described previously, a four-vessel occlusion method was utilized to induce global cerebral ischemia [37]. All procedures in our study were performed under aseptic conditions. Briefly, anesthesia was induced with 3–4% isoflurane at 3 L/min in 100% oxygen in a chamber and maintained during the operation with a mask using 2–3% isoflurane at 800 ml/min in 100% oxygen. Vertebral arteries were occluded by electrocauterization. After isolated bilateral common carotid arteries, a teflon/silastic occluding device was placed loosely around each carotid artery without interrupting blood flow. Then global cerebral ischemia was induced for 10 min at 24 h after surgery in awake rats, by occluding both common carotid arteries. After occlusion, rats that lost their righting reflex within 1 min with dilated pupils were selected for the following experiments. Rectal temperature was maintained at 37°C throughout the experiment. Sham-operated (Sham) rats received the same surgical procedures without 10-min occlusion of common carotid arteries. Rats that convulsed during ischemia or post-ischemia were excluded from this study.

Twenty-four hours after ischemia, rats were placed in a hypoxic chamber, through which air containing 8% O_2 and 92% N_2 flowed continuously at a temperature of 23–25°C for 120 min to implement HPC [35]. Sham-operated, hypoxia treated rats were exposed to 120-min hypoxia 24 h after sham-operated procedures without ischemia.

2.3 | Administration of drugs

Implantation of the intracerebroventricular injection into the right lateral ventricle (1.5 mm lateral, 0.8 mm posterior and 4.0 mm dorsal with respect to the bregma) was performed stereotaxically after isoflurane anesthesia. Cannula was affixed to the skull with stainless steel screws and cranioplastic cement. Rats were arranged to recover from surgery for 1 week before treatment. All animals displayed normal feeding and drinking behaviors postoperatively.

Sequences for Piwil2 antisense oligodeoxynucleotide (AS-ODN) (5′-GGUCGGGUUGAUCACCACAACUAG-3′) were referenced to the report by Rajasethupathy et al [10]. AS-ODN was synthesized with a phosphorothioate backbone, purified by ULTRAPAGE (Sangon, Inc. Shanghai, China) and dissolved with artificial cerebrospinal fluid (aCSF). A solution containing 10 μl of AS-ODN (5 μmol/L) or aCSF was injected over a 10-min period each time intracerebroventricularly at 24 h before tGCI and immediately after tGCI. For Sham rats, AS-ODN or aCSF was administrated twice at the same time point in 2 d after operation.

2.4 | Analysis of cellular damage

Animals after chloral hydrate (350 mg/kg i.p.) anesthesia were perfused intracardially with normal saline, followed by 4% paraformaldehyde in PBS at 168 h after cerebral ischemia. Brains were removed quickly and postfixed in 10%, 20%, and 30% sucrose in the same fixative for cytoprotection. Then brains were frozen at −20°C and sliced into coronal 30 μm-thick sections with a cryotome (Leica, Wetzlar, Germany). Sections selected from the dorsal hippocampus [between anterior–posterior (AP) 4.8 and 5.8 mm, interaural or AP- 3.3 to 3.4 mm, Bregma] were used. To determine the hippocampal cellular damage, Nissl, neuronal nuclei (NeuN), and Fluoro-Jade B (FJ-B) staining were conducted as described previously [35]. Briefly, Nissl staining was performed with 0.1% cresyl violet (MilliporeSigma, Burlington, MA), and then sections were dehydrated with 90% and 100% ethanol and immersed into dimethylbenzene. For FJ-B staining, sections were immersed in 70% ethanol, washed with distilled water, and treated with 0.06% potassium permanganate solution for 10 min. Then, the sections were incubated with 0.004% FJ-B (MilliporeSigma) in 0.1% acetic acid for 20 min, washed, and mounted with distrene plasticizer xylene (MilliporeSigma).

The sections from Nissl and NeuN staining were examined under a light microscope with ×660 magnification. FJB stained images were observed with a fluorescent microscope (Leica Microsystems, Wetzlar, Germany). As described previously [38], cells in the CA1 pyramidal layer were quantitatively analyzed within three nonrepeated rectangular areas of 0.037 mm^2. Data were quantified bilaterally in four sections from each rat and assessed blindly.

2.5 | Immunohistochemistry

Animals were sacrificed at 0, 4, 26, 50, and 168 h after reperfusion of tGCI with or without hypoxia. Single-

labeled immunohistochemistry was performed using the avidin-biotin complex peroxidase method [35]. Briefly, the sections were first treated with 3% hydrogen peroxide for 30 min, followed by 5% normal serum for 1 h, and then, they were incubated overnight at 4°C with primary antibodies including Piwil2 (1:500; Abcam, Cambridge, United Kingdom, Cat# ab36764) and NeuN (1:6000; MilliporeSigma). Immunopositive cells in which the reaction product was present within a clear and regular-shaped cytoplasmic or nuclear border were quantified under a light microscope with ×660 magnification. The number of immunopositive cells was counted by the total number of four nonrepeated random fields (0.037 mm^2/field × 4 = 0.148 mm^2 in total) in the CA1 subregions. Data were quantified bilaterally in four sections from each rat and assessed blindly.

Double-fluorescent immunohistochemistry was utilized to observe the exact location of Piwil2. NeuN, microtubule-associated protein-2 (MAP-2), and glial fibrillary acidic protein (GFAP) were used to identify neuronal nuclei, neuronal cell bodies and dendrites, and astrocytes, respectively. Double-fluorescent immunohistochemistry was performed as described previously [39]. Antibodies used in these studies included Piwil2 (1:200; Abcam, Cat# 85084), NeuN (1:1000; MilliporeSigma), MAP-2 (1:1000; MilliporeSigma), GFAP (1:3000; MilliporeSigma), Cy3-conjugated goat anti-mouse IgG antibody (1:100; Abcam), and FITC-conjugated goat anti-rabbit IgG antibody (1:100; Abcam). Slides were mounted with mounting medium containing 4′, 6-diamidino-2-phenylindole (DAPI, Solarbio, Beijing, China) and analyzed with a confocal laser microscope (SP8, Leica Microsystems, Wetzlar, Hessen, Germany).

2.6 | Western blotting

Rats were sacrificed at 0, 4, 26 and 50 h after reperfusion of tGCI with or without hypoxia. The brain samples were cut into 2 mm coronal slices using a brain matrix, and the CA1 subregion of bilateral hippocampi were quickly dissected under a stereomicroscope. Proteins of CA1 were extracted as previously described [39]. Western blot was performed as previously described [39] with the primary antibodies including Piwil2 (1:500; Abcam, Cat# ab36764), CREB2 (1:500; Abcam), cleaved caspase-3 (1:800; Cell Signaling Technology, Beverly, MA), cleaved-caspase-9 (1:1000; Cell Signaling Technology), DNMT3A (1:500; Cell Signaling Technology), β-Tublin (1:10000; MilliporeSigma) and glyceraldehyde 3-phosphate dehydrogenase (GADPH; 1:10,000; Proteintech Group, Chicago, IL). Densitometric analysis for the quantification of the bands was performed with image analysis software (Quantity One, Bio-Rad Laboratories, Hercules, CA). Relative optical densities of protein bands were calibrated with β-Tublin or GADPH and normalized to those in Sham rats.

2.7 | Isolation of total RNA and reverse transcription quantitative real-time polymerase chain reaction (RT-qPCR)

Total RNA was extracted from the CA1 subregion using Trizol reagent (Invitrogen, Carlsbad, CA). RT-qPCR was performed according to the standard protocol. For each sample, 1 μg of RNA was reverse-transcribed into cDNA in a final volume of 20 μl with 1 μl primer mix, 4 μl buffer and 1 μl enzyme mix (Takara, Shiga, Japan). The primers used are as follow: Piwil2: 5′-ATGGAGTAGAATGCTGGGAA-3′(forward), 5′-CCTTGCTTGACCAAAAGCTC-3′(reverse), CREB2: 5′-TCGATGCTCTGTTTCGAATG-3′(forward), 5′-GGCAACCTGGTCGACTTTTA-3′(reverse), β-actin: 5′-GCGTCCACCCGCGAGTACAA-3′(forward), 5′-TCCATGGCGAACTGGTGGCG-3′(reverse) (Sangon Biotech, Shanghai, China). Afterwards, PCR was performed in a final volume of 25 μl with 2 μl of RT product for cDNA amplification. Annealing temperature was 60°C. Quantitative PCRs were conducted by LightCycler Fast-Start DNA Master SYBR Green 1 kit and on a LightCycler 1.5 PCR machine (Roche Light Cycler 480, Germany). Each sample was run in triplicates. All of the samples were quantified against the same standard curve, and each expression level was normalized to β-actin expression. Data were analyzed using the comparative C_t method ($2^{-\Delta\Delta Ct}$). Results were expressed as fold changes compared to Sham group.

2.8 | Small RNA sequencing, target prediction and functional analyses

Small RNA sequencing service was provided by Cloud-Seq Biotech Ltd. Co. (Shanghai, China). Briefly, samples were collected from bilateral hippocampal CA1 region as genomic source (n = 3 in each group). Total RNA of each sample was prepared using Trizol reagent (Invitrogen), and the RNA quality and integrity were confirmed. 5′- and 3′-Adaptors were ligated to the obtained small RNA. Reverse transcription followed by PCR was used to create cDNA constructs. Subsequently, an about 150 bp fraction corresponding to approximate the adaptor-ligated constructs derived from the 30 nts piRNA fragment was excised and purified. The purified libraries were sequenced on Illumina HiSeq 2000 apparatus. The raw data were refined using cutadapt software (v1.9.1). After filtering out low quality reads and short reads (<15 nts), trimmed reads from all samples were pooled, and piano software was used to predict novel piRNAs. The trimmed reads were aligned to the merged rat piRNA databases (known piRNA from piRNABank plus the newly predicted piRNAs) using Novoalign software (v3.02.12) with at most one mismatch. PiRNA-binding transposon and targets were predicted by miranda software (v3.3a). piRNA-targets networks were

plotted by cytoscape software (v2.8.0). Pathways and Gene Ontology (GO) classification were analyzed based on the Kyoto Encyclopedia of Genes and Genomes (KEGG) database and GO database.

2.9 | RNA binding protein immunoprecipitation (RIP) assay

To identify Piwil2-interacting piRNAs, samples from CA1 subregion ($n = 3$ in each group) were lysed in 500 μl lysis buffer and centrifuged. After centrifugation, supernatant was incubated with monoclonal mouse antibody against Piwil2 (Santa Cruz, California, CA), preincubated with Protein A/G Agarose. The beads were washed twice with lysis buffer. After quality check by Western blot, the RNA was extracted from the magnetic beads using Trizol reagent (Invitrogen). Then, the immunoprecipitated RNA was analyzed with small RNA sequencing.

2.10 | DNA methylation assays

DNA methylation assays were performed by methylation-specific PCR (MSP) and bisulfite sequencing PCR (BSP). Genomic DNA was extracted from hippocampal CA1 subregion using universal genomic DNA extraction kit (Blood&Tissue kit, 69504; Qiagen, Germany). Purified DNA was then processed for bisulfite modification (EpiTect Bisulfite Kit, 59104; Qiagen). Bisulfite treatment of genomic DNA converts cytosine to uracil, leaving methylated 5-cytosines unchanged. MSP ($n = 3$ in each group) on -the CpG islands of the *CREB2* were performed with the unmethylation-specific primers and methylation-specific primers. The primer sequences, external primer: 5′-ATAGTTTTGGTTAGGTGTTTTTTTA-3′(forward), 5′-CTACCACAAAACAAACAAAAAT-3′(reverse); internal primer: primers of methylation: 5′-GTTTTGGTTAGGT GTTTTTTTACGT-3′(forward), 5′-CCTTCTCCGCTA-TACTCGAA-3′(reverse); primers of unmethylation: 5′-AGTTTTGGTTAGGTGTTTTTTTATGT-3′(forward), 5′-CAAACCCTTCTCCACTATACTCAAA-3′(reverse). The products of amplification were analyzed with agarose electrophoresis. BSP analysis was provided by Sangon Biotech Ltd. Co. (Shanghai, China). The primer sequences used for BSP were: 5′-TTTTTYGATATTAGTGTTTTTAG GG-3′(forward), 5′-CACCTAACCCTATCCCATTAAC-3′ (reverse). The PCR products were then sequenced using an automated sequencer ABI 3730XL (Applied Biosystems, Foster City, CA).

2.11 | Lentivirus construction and lentiviral administration

Plasmids containing the sequence of rat *Piwil2* (GenBank accession number NM_001107276) and a negative control sequence (CON235) were designed by Genechem (Shanghai, China). The sequence was inserted into AgeI and AgeI sites of the Ubi-MCS-3FLAG-CMV-EGFP (GV365) lentiviral vector. The shuttle vector and viral packaging system were cotransfected into HEK293T cells to produce recombinant lentiviruses using Lipofectamine 2000 (Invitrogen). Then HEK293T cells were used for viral infection. The infection efficiency was greater than 80%, as monitored with GFP protein expression. After 48 h of infection with lenti-*Piwil2*, the cells were harvested, and total RNA was extracted to examine the expression of Piwil2 mRNA. The titers were approximately 1×10^9 TU/ml.

Lentiviral administration was carried out as described previously [38]. Briefly, a total of 5 μl volume (1.25 μl virus diluted by 3.75 μl enhanced solution) containing 1.25×10^9 TU/ml of particles was injected into bilateral hippocampal CA1 region (3.5 mm posterior to bregma, 2.3 mm lateral to bregma, and 2.6 mm below the dura) using a 10-μl Hamilton syringe with 34-gauge needle at a flow rate of 0.3 μl/min. The rats were arranged to recover for up to 14 d to enable sufficient gene expression.

2.12 | Golgi staining, cell selection and imaging analysis

Rats were first intracardially perfused with saline that was followed by a quick removal of the brains. The rapid Golgi staining was performed by using the FD Rapid GolgiStain kit (FD Neurotechnologies Inc, Columbia, MD). After impregnating and fixing the tissues for 2 weeks, the brain was cut into 100 μm using a vibratome (Zeiss Axio Imager M2, Germany) at −22°C. Following drying, the sections were stained with appropriate solutions of the kit. After dehydrating in increasing concentrations of alcohol and clearing in xylene, the sections were coverslipped with permount mounting medium and kept in a dark place.

The pyramidal cells of the CA1 from bilateral dorsal hippocampi were selected. The criteria for selection of neurons were as follows: (1) cells located in the middle part of the section to avoid their branches being cut off, (2) distinct and consistent impregnation throughout the whole cell, and (3) relative isolation from neighbors to avoid overlapping dendrites of adjacent cells. Generally, 5–8 neurons in each CA1 region which meet the selection criteria were chosen for each animal. All of the measurements were double checked by two researchers independently.

Photomicrographs were generated with a Leica Imaging System. Sequential 2D reconstructions of entire dendritic tree were generated by Image Pro 5.0. Total dentritic length of the pyramidal cells, including both basal and apical dendrites, was analyzed. The dendritic tracings were quantified by Sholl analysis [40]. A transparent grid with equidistant (10 μm) concentric rings was centered over the

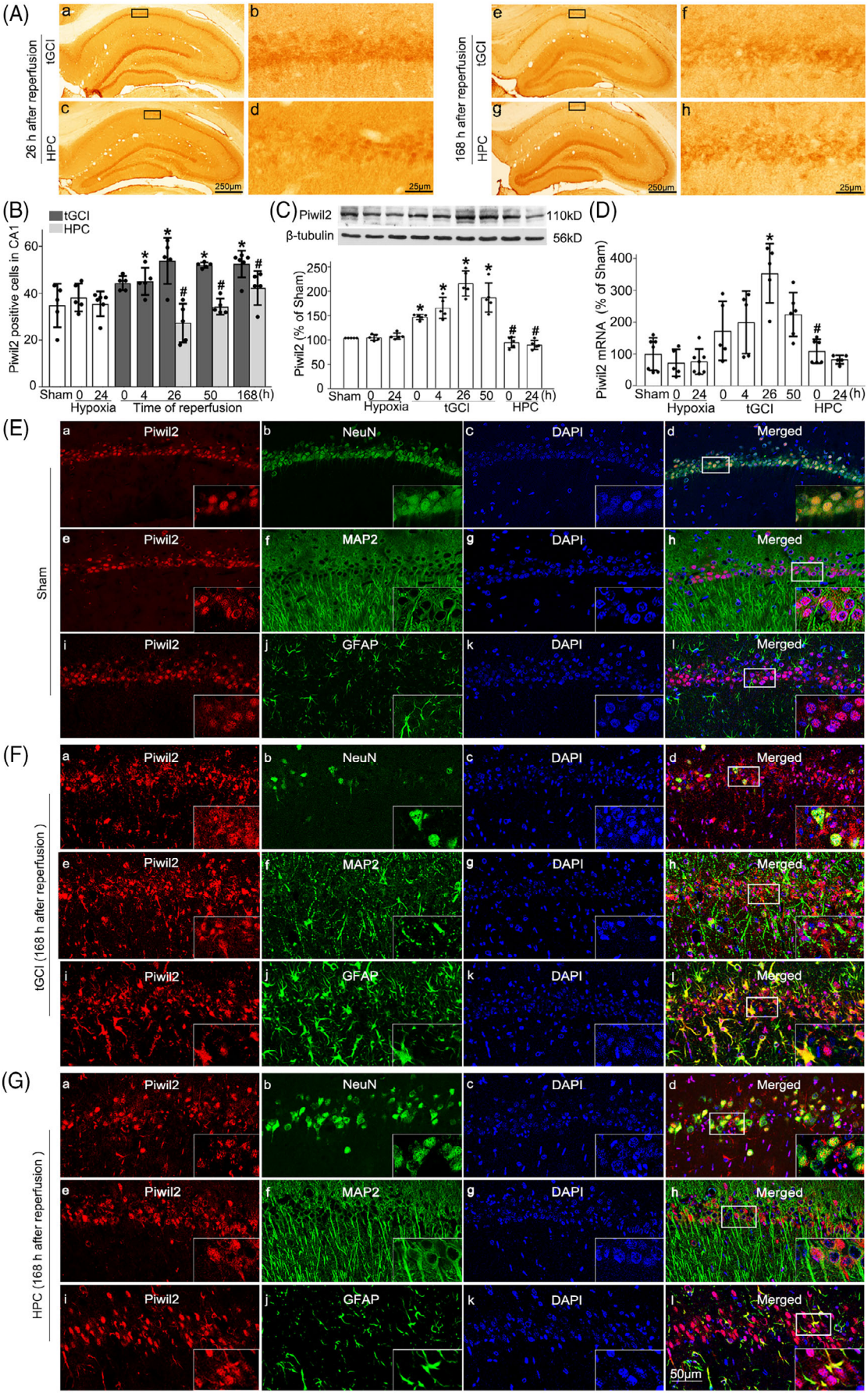

FIGURE 1 Legend on next page.

dendritic tree tracings and the number of ring intersections was used to estimate the dendritic arborization. The density of dendritic spines was estimated by randomly selecting high-magnification tracings (×100 immersion objective) of a terminal segment from the basal and apical dendrite branches [40]. The selection of basal and apical dendrites was according to the ratio 1:1. Spine density was estimated by counting the number of visible spines along the branch segment. Spine density was calculated as average number of spines per 10 μm of dendrite [41].

2.13 | Morri water maze

The Morris water maze was performed by an investigator who was blinded to the experimental groups. The aquatic maze consists of a circular black pool (210 cm in diameter, 60 cm in height; Taimeng Technology Co., Ltd, Chengdu, China) filled with opaque water (20 cm in depth, 23 ± 1°C), which was divided into four equal-sized quadrants (Q1, Q2, Q3, and Q4). The pool had a transparent platform (escape platform) (10 cm in diameter) which was placed 2.0 cm below the water surface in Q1.

Rats were put into the pool facing toward the wall and every starting point was used in a different order each day. Starting positions were designated as Q1, Q2, Q3, or Q4. All rats were trained to find the hidden platform within a maximum time limit of 120 s and then allowed to remain on the platform for 15 s. If the rat failed to find the platform, it was guided to there, and the escape latency was recorded as 120 s. The platform remained in the same location throughout the training period. All rats were subjected to four consecutive trials per day at 10 min intervals for five consecutive days from the 2nd day after tGCI. The path length, the escape latency and swimming speed for each trial were recorded.

Twenty-four hours after the end of a training period, a 30-s probe trial without the platform was conducted to evaluate the long-term memory. All rats were placed in maze at a fixed starting point (the most distance to the platform position used during the training period). The time in the target quadrant occupancy was also recorded at day 7 after tGCI.

All tests were almost conducted at the same time each day in order to minimize variability in performance of rats. The parameters for each trial were recorded with a video tracking system (SMART, Polyvalent video-tracking system, 35B73-C6C, PANLAB, Spain).

2.14 | Data analyses

Statistical analyses were performed with the Statistical Package for Social Sciences for Windows, version 13 (SPSS, Inc, Chicago, Illinois). Data were expressed as mean ± SD. Two-way ANOVA was used to compare the numbers of positive cell or the optical densities of protein band between HPC and tGCI groups. One-way ANOVA analysis was used to compare the numbers of positive cell or the optical densities of protein band between tGCI and Sham groups. Analyses were followed by a Bonferroni or Tamhane's T2 post hoc test. Values of $p < 0.05$ were considered statistically significant.

3 | RESULTS

3.1 | The downregulation of Piwil2 in CA1 induced by HPC contributes to the neuroprotection against tGCI

We first analyzed the protein and transcription levels of Piwil2 in CA1 of rats after tGCI with and without hypoxia (Figure 1A–D). Compared with Sham rats, tGCI induced a sustained elevation of Piwil2 in CA1 after reperfusion. In contrast, HPC dramatically attenuated the tGCI-induced elevation of Piwil2, which was detected by immunohistochemical assay and Western blot (Figure 1A–C). Meanwhile, Piwil2 mRNA was expressed at a high level at 26 h of reperfusion after tGCI. Interestingly, HPC completely prevented the tGCI-induced elevation of Piwil2 mRNA (Figure 1D). As shown in Figure 1E, double-fluorescent immunohistochemistry revealed that Piwil2 were colocalized with NeuN, and surrounded by MAP-2-potitive cells in CA1 of Sham animals, indicating that Piwil2 has predominant nuclear location in neurons. Additionally, at 168 h after tGCI, most of Piwil2-positive cells co-lapped with GFAP were indicated as astrocytes (Figure 1F), whereas in HPC rats the majority of Piwil2-positive cells co-labeled with NeuN were located in neurons (Figure 1G).

FIGURE 1 HPC prevents the tGCI-induced upregulation of Piwil2 in CA1. (A) Immunohistochemistry of Piwil2 in the hippocampus of rats. Representative microphotographs show 26 h after reperfusion of tGCI groups (a, b) and HPC groups (c, d), 168 h after reperfusion of tGCI groups (e, f) and HPC groups (g, h), respectively. (B) Quantitative analysis of Piwil2-immunoreactivities in CA1. (C) Western blot analysis of Piwil2 expression in CA1. The histogram presents the quantitative analyses of Piwil2. (D) RT-qPCR analysis of Piwil2 mRNA in CA1. Data are expressed as percentage of value of Sham animals. Each bar represents the mean ± SD. $^{*}p < 0.05$ vs. Sham animals and $^{\#}p < 0.05$ vs. tGCI groups at the same time point. (E–G) Representative photomicrographs with fluorescent staining of Piwil2 (red), NeuN/MAP-2/GFAP (green) and DAPI (blue) in CA1. The overlapped images show that Piwil2 was prominently colocalized with NeuN and surrounded by MAP-2-potitive cells in CA1 of Sham animals (E). Piwil2-positive cells mainly co-lapped with GFAP in CA1 at 168 h after tGCI (F). Piwil2 in CA1 at 168 h in the HPC groups mostly located in NeuN and partially in GFAP-positive cells (G). DAPI, 4′,6-diamidino-2-phenylindole; GFAP, glial fibrillary acidic protein; HPC, hypoxic postconditioning; MAP-2, microtubule-associated protein-2; NeuN, neuronal nuclei; Sham, sham-operated; tGCI, transient global cerebral ischemia

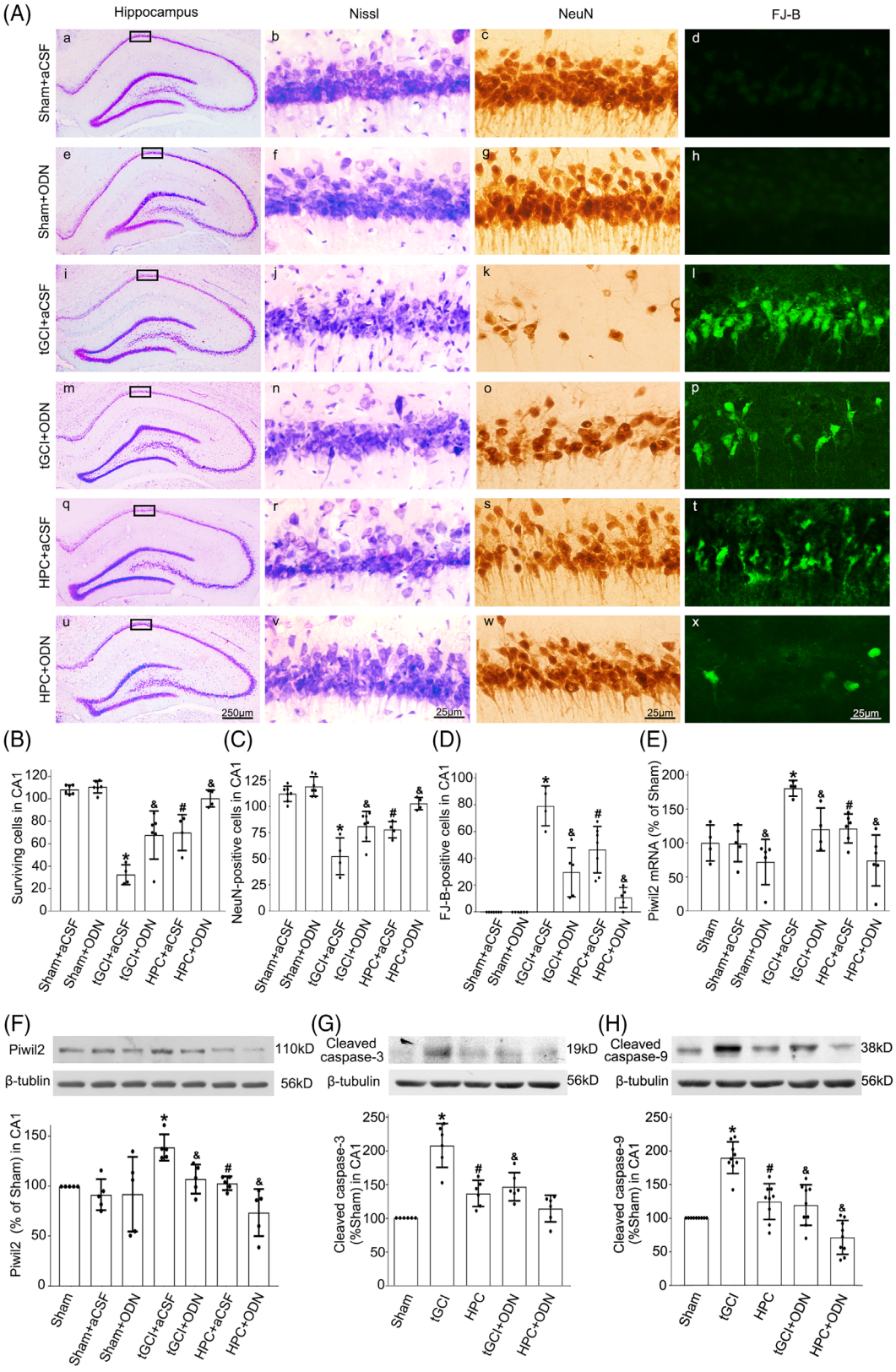

FIGURE 2 Legend on next page.

To test the potential function of Piwil2 in the neuroprotection mediated by HPC after tGCI, we examined the effects of Piwil2 knockdown or overexpression on neuronal damage. As expected, the intraventricular injection of aCSF or Piwil2 AS-ODN had no impact on the pyramidal neurons in CA1 of Sham rats. However, Piwil2 AS-ODN

administration markedly ameliorated neuronal damage in CA1 after tGCI. In addition, a cumulative neuroprotective effect was observed when HPC and Piwil2 AS-ODN were combined (Figure 2A–D). As shown in Figure 2E,F, the administration of Piwil2 AS-ODN significantly reduced both the transcription and protein levels of Piwil2 at 26 h after tGCI with and without hypoxia. Meanwhile, the injection of Piwil2 AS-ODN reduced the levels of cleaved caspase-3 and caspase-9 in CA1 at 26 h after tGCI (Figure 2G,H). Differing results were obtained after the administration of Piwil2-carried lentivirus (referred to as Lenti-*Piwil2*) into the bilateral hippocampus (Figure 3). Rats were randomly subjected to sham-operation or tGCI 14 d after the administration of Lenti-*Piwil2* or scrambled lentivirus vector (referred to Lenti-Control) (Figure 3A). Fluorescent images confirmed the effective transfection of lentivirus in CA1 (Figure 3B). Double-labeled immunofluorescent studies showed that Piwil2 was colocalized with GFP in lenti-*Piwil2*-administrated rats (Figure 3C). In addition, lenti-*Piwil2* administration did not alter neuronal cell number in CA1 of Sham rats, but abolished HPC-induced neuroprotection as evidenced by a dramatic decrease in the number of surviving cells and NeuN-positive cells in CA1 (Figure 3D–F). Accordingly, the expression of Piwil2 in CA1 detected by Western blot substantially increased at 26 h of reperfusion after the administration of lenti-*Piwil2* either in Sham or HPC rats (Figure 3G).

3.2 | The Piwil2/piRNAs pathway regulated by HPC downregulates the expression of DNMT3A in CA1 after tGCI

To evaluate the effect of tGCI with HPC on piRNA expression profiles, small RNA sequencing was performed. Hierarchical clustering showed systematic variations in the expression of piRNAs between tGCI and HPC brains (Figure S1A,B). The differentially expressed piRNAs in CA1 were mainly clustered in axon guidance and synaptic functions (Figure S1C). After tGCI, a total of 5574 piRNAs in CA1 was detected after 26 h of reperfusion. Of those, 12 were significantly upregulated compared with Sham rats (≥1.5-fold change, $p < 0.05$), including 6 novel piRNAs. Of the 12 piRNAs, 4 showed ≥2-fold change. In comparison to tGCI group, 6 piRNAs in CA1 were significantly downregulated after HPC. Interestingly, the piRNAs rno_piR_000618, rno_piR_017990 and rno_piR_014971 were significantly changed in both tGCI and HPC groups (Figure S1D). Also, we observed CREB2 targeted by three piRNAs, rno_piR_000618, rno_piR_017990, and rno_piR_014971 (Figure S1E). All sequencing data have been deposited into the Gene Expression Omnibus (GEO) database under the accession number GSE163298.

To evaluate the profiles of Piwil2-interacting piRNAs in CA1, RIP was performed. All data is available in the GEO database (GEO accession number GSE163299). Hierarchical clustering showed systematic variations in the expression of Piwil2-interacting piRNAs between tGCI and HPC brains (Figure 4A,B). The differentially expressed Piwil2-interacting piRNAs in CA1 were mainly clustered in axon guidance and synaptic functions (Figure 4C). As shown in Figure 4D, after tGCI, a total of 423 Piwil2-interacting piRNAs in CA1 was upregulated after 26 h of reperfusion. Of the 423 piRNAs, 317 were significantly upregulated by more than 1.5-fold. Of the 317 piRNAs, 258 showed ≥2-fold change. A comparison between tGCI and HPC groups revealed that 401 Piwil2-interacting piRNAs in CA1 were significantly downregulated after HPC, whereas only seven piRNAs were found to be altered in all three groups studied (≥1.5-fold change). In order to illuminate the function of Piwil2/piRNAs in neuroprotection induced by HPC against tGCI, the target genes of the Piwil2-interacting piRNAs were predicted, and the GO term and KEGG analyses were conducted based on the targets of differentially expressed piRNAs between HPC and tGCI groups. The results of the prediction showed that DNMT3A may be a potential common target of the seven differentially expressed Piwil2-interacting piRNAs (Figure 4E). Therefore, we focused on examining the expression of DNMT3A in CA1 after tGCI with and without hypoxia. As shown in Figure 5A, DNMT3A was significantly upregulated at 4 h postischemia, and this upregulation persisted through 50 h in CA1 after tGCI, whereas HPC decreased DNMT3A levels in CA1 after tGCI. Further, we found that Piwil2 knockdown by AS-ODN would lead to a marked reduction of DNMT3A

FIGURE 2 Silencing of Piwil2 inhibits the expression of cleaved caspase proteins and alleviates tGCI-induced neuronal damage in CA1. (A) Representative microphotographs of cresyl violet staining, immunostaining of NeuN, and FJ-B staining in the hippocampus at 7 d after tGCI with and without Piwil2 AS-ODN administration. Sham + aCSF group (a–d), injection with aCSF without ischemia or hypoxia; Sham + ODN group (e–h), injection with Piwil2 AS-ODN without ischemia or hypoxia; tGCI + aCSF group (i–l), injection with aCSF at 24 h before tGCI and immediately after tGCI; tGCI + ODN group (m–p), injection with Piwil2 AS-ODN at 24 h before tGCI and immediately after tGCI; HPC + aCSF group (q–t), injection with aCSF at 24 h before tGCI and immediately after tGCI; HPC + ODN group (u–x), injection with Piwil2 AS-ODN at 24 h before tGCI and immediately after tGCI. (B–D) quantitative analyses of surviving cells, NeuN and FJ-B positive cells in CA1. (E) RT-qPCR analysis of Piwil2 mRNA in CA1 after tGCI with and without Piwil2 AS-ODN administration. (F–H) Representative images of Western blot show the expression of Piwil2, cleaved caspase-3 and cleaved caspase-9 in CA1 after tGCI with and without Piwil2 AS-ODN administration. The histogram presents the quantitative analyses of Piwil2, cleaved caspase-3 and cleaved caspase-9 in CA1. Data are expressed as percentage of value of Sham animals. Each bar represents the mean ± SD. $^{*}p < 0.05$ vs. Sham animals, $^{\#}p < 0.05$ vs. tGCI group and $^{\&}p < 0.05$ vs. tGCI group or HPC group administrated with aCSF. aCSF, artificial cerebrospinal fluid; AS-ODN, antisense oligodeoxynucleotide; FJ-B, Fluoro-Jade B; HPC, hypoxic postconditioning; NeuN, neuronal nuclei; Sham, sham-operated; tGCI, transient global cerebral ischemia

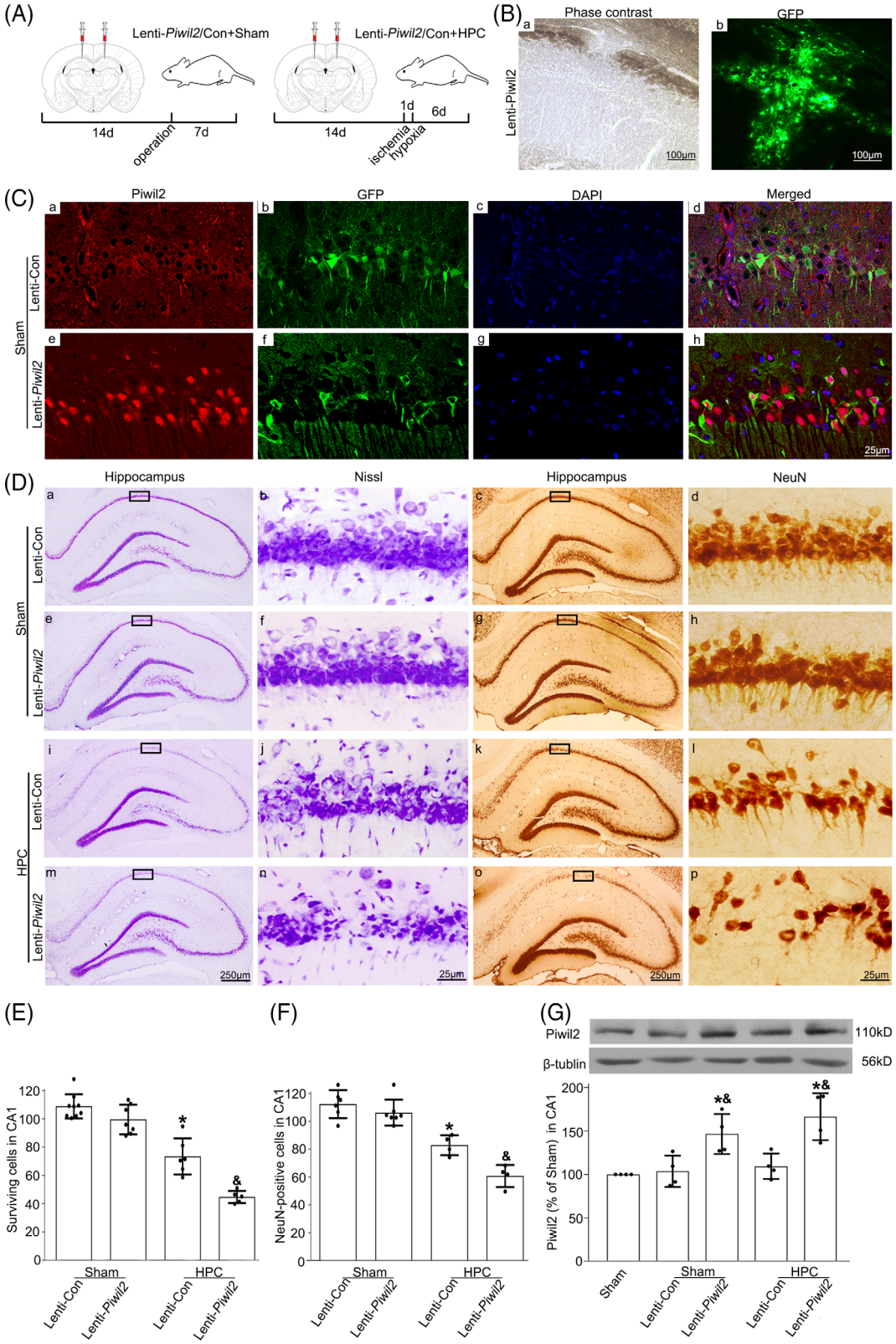

FIGURE 3 Legend on next page.

expression in CA1 after tGCI with and without hypoxia (Figure 5B), while the overexpression of Piwil2 in CA1 significantly increased the DNMT3A expression either in Sham or HPC rats (Figure 5C). These data suggested that the Piwil2/piRNAs pathway regulated by HPC may target to DNMT3A and the downregulation of Piwil2

induced by HPC reduces the level of DNMT3A protein in CA1 after tGCI.

3.3 | The downregulation of Piwil2 induced by HPC increases the expression of CREB2 through inhibiting DNA methylation in CA1 after tGCI

As shown in Figure 5D, the levels of CREB2 protein in tGCI increased at 4 h, peaked at 26 h, and began to decrease at 50 h after reperfusion. In contrast, HPC maintained the higher level of CREB2 in CA1 after tGCI. Accordingly, the levels of CREB2 mRNA were significantly upregulated in CA1 from 0 h to 4 h after reperfusion but decreased at 26 h and then returned to basal level at 50 h in tGCI rats. Notably, HPC completely prevented the tGCI-induced reduction of CREB2 mRNA at 26 h of reperfusion (Figure 5G). To determine the correlation between CREB2 and Piwil2 in the roles of cerebral ischemia, we detected the alteration in CREB2 expression in CA1 regulated by Piwil2. More interestingly, the knockdown of Piwil2 with AS-ODN induced the increases in the mRNA and protein levels of CREB2 in tGCI rats with and without hypoxia (Figure 5E,H). Consistently, when Piwil2 was overexpressed with lenti-*Piwil2* administration in HPC rats, the expression of CREB2 was inhibited at 26 h of reperfusion (Figure 5F).

In view of the roles of Piwi/piRNAs in epigenetic regulation through DNA methylation, we investigated whether CREB2 is being regulated by Piwil2 depending on methylation at its promoter. As shown in Figure 5I, a predicted CpG island locates at 1540 bp to 1943 bp proximal to the upstream of the first exon of the *CREB2* promoter (873 bp upstream of the first ATG) was found. The results of MSP showed that the *CREB2* promoter exists in both methylated and unmethylated forms in CA1 of Sham rats. Compared to Sham group, this methylated signal in CA1 was stronger in tGCI and weaker in HPC rats (Figure 5J). In the region of CpG island at the *CREB2* promoter, 331 CpG methylation sites were detected using BSP. Our data showed that almost each CpG site in the *CREB2* promoter exists in about 0.6% methylated form in CA1 of Sham rats. Interestingly, after exposure to tGCI, the frequency of methylation at each CpG site of *CREB2* promoter increased to 1.67% ± 0.33%. As expected, this increase in methylation of CREB2 after tGCI dropped to below the baseline after HPC (Figure 5K). To investigate whether Piwil2 was required for the hypermethylation of CREB2 in CA1 after tGCI, As-ODN was employed to inhibit Piwil2, and the result showed that the tGCI-induced increase in methylation at the promoter of CREB2 in CA1 was abolished (Figure 5J,K).

3.4 | The downregulation of Piwil2 induced by HPC enhances the plasticity of hippocampal dendritic spines and improves memory function after tGCI

To determine whether HPC affects dendritic structure in hippocampus, Golgi staining was used to examine the alterations in dendrite complexity and spine density in hippocampal neurons at 50 h after reperfusion. We observed that dendrites in CA1 pyramidal neurons were severely distorted, with a bead-like appearance and collapsed down into the dendritic shaft after tGCI, but they were partially restored when applied with HPC or Piwil2 knockdown (Figure 6A). Interestingly, analysis of dendritic branch trees of CA1 neurons using Sholl analyses revealed that the mean number of dendritic branch intersections in the CA1 neurons were more in the groups with HPC or AS-ODN administration than those in the tGCI with aCSF treatment (Figure 6C). Particularly, HPC with aCSF administration increased the number of dendritic branch crossings from 80 to 200 μm away from the cell soma compared to tGCI with aCSF administration rats (Figure 6B). We further analyzed dendritic spine morphology in CA1 pyramidal neurons (Figure 6D,E). The tGCI rats with aCSF treatment showed significant reduction in the dendrite length and total spine density compared with Sham rats. By contrast, HPC with aCSF administration or knockdown of Piwil2 with AS-ODN administration restored dendrite length and total spine density after tGCI.

FIGURE 3 Overexpression of Piwil2 reverses the HPC-induced neuroprotection in CA1 after tGCI. (A) Design of experiments in which rats were stereotaxically injected bilaterally with *Piwil2* lentiviral vectors in the dorsal CA1 pyramidal layer and subjected to either Sham or tGCI with hypoxia. (B) Phase contrast and fluorescent images from coronal sections of CA1 following injection of *Piwil2* lentiviral vectors in Sham animals. (C) Representative photomicrographs show the colocalization of Piwil2 (red), GFP (green) and DAPI (blue) in CA1 from Sham animals with Lenti-*Piwil2* injection. (D) Cresyl violet stained and NeuN immunostained hippocampal sections from rats administered bilaterally with either Lenti-Control or Lenti-*Piwil2* at 7 d after reperfusion with hypoxia. Boxes indicate that the magnified regions displayed in the right panel. (E,F) Quantitative analyses of surviving cells and NeuN-positive cells in CA1. Each bar represents the mean ± SD. $^{*}p < 0.05$ vs. Sham + Lenti-con animals, and $^{\&}p < 0.05$ vs. HPC group with injection of Lenti-Con. (G) Representative immunoblots of Piwil2 expression in CA1 after HPC with and without *Piwil2* lentiviral vectors administration. The histogram presents the quantitative analyses of Piwil2 protein. Data are expressed as percentage of value of Sham animals. Each bar represents the mean ± SD. $^{*}p < 0.05$ vs. Sham animals, and $^{\&}p < 0.05$ vs. Sham or HPC group with injection of Lenti-Con. DAPI, 4′,6-diamidino-2-phenylindole; HPC, hypoxic postconditioning; NeuN, neuronal nuclei; Lenti-Con, Lenti-Control: scrambled lentivirus vector; lenti-*Piwil2*, *Piwil2*-carried lentivirus; Sham, sham-operated; tGCI, transient global cerebral ischemia

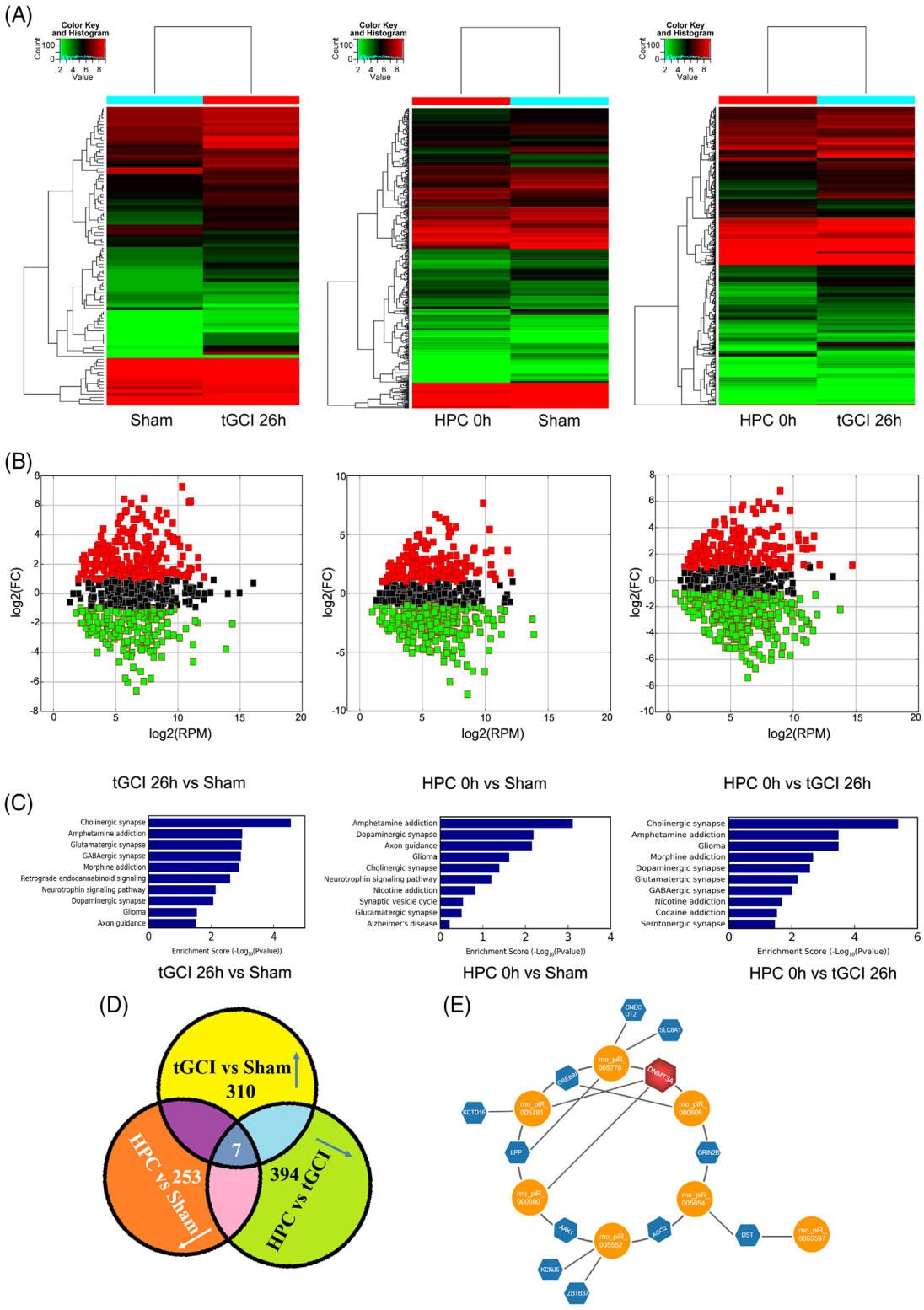

FIGURE 4 Aberrant expression of Piwil2-interacting piRNAs in hippocampal CA1 of rats after tGCI with and without hypoxia. (A) Heatmap generated from hierarchical cluster analysis shows the differential expressed Piwil2-interacting piRNAs in CA1 between tGCI and HPC groups. Green indicates downregulation and red indicates upregulation. (B) The differential expression of Piwil2-interacting piRNAs in CA1 between tGCI and HPC groups. *Y*-axis: fold-change (FC); *X*-axis: Reads per million mapped reads (RPM); green indicates downregulation and red indicates upregulation. (C) Gene-enriched KEGG analysis of deferentially expressed Piwil2-interacting piRNAs in CA1 of tGCI and HPC groups. (D) The Venn diagram shows a comparison of differentially expressed Piwil2-interacting piRNAs among Sham, tGCI and HPC groups (≥1.5-fold change). (E) The network of piRNA-target interactions. PiRNAs are shown in orange nodes, and genes are shown in blue nodes. The red node is the common target of the selected seven Piwil2-interacting piRNAs that were observed to be altered in all three groups studied. HPC, hypoxic postconditioning; Sham, sham-operated; tGCI, transient global cerebral ischemia

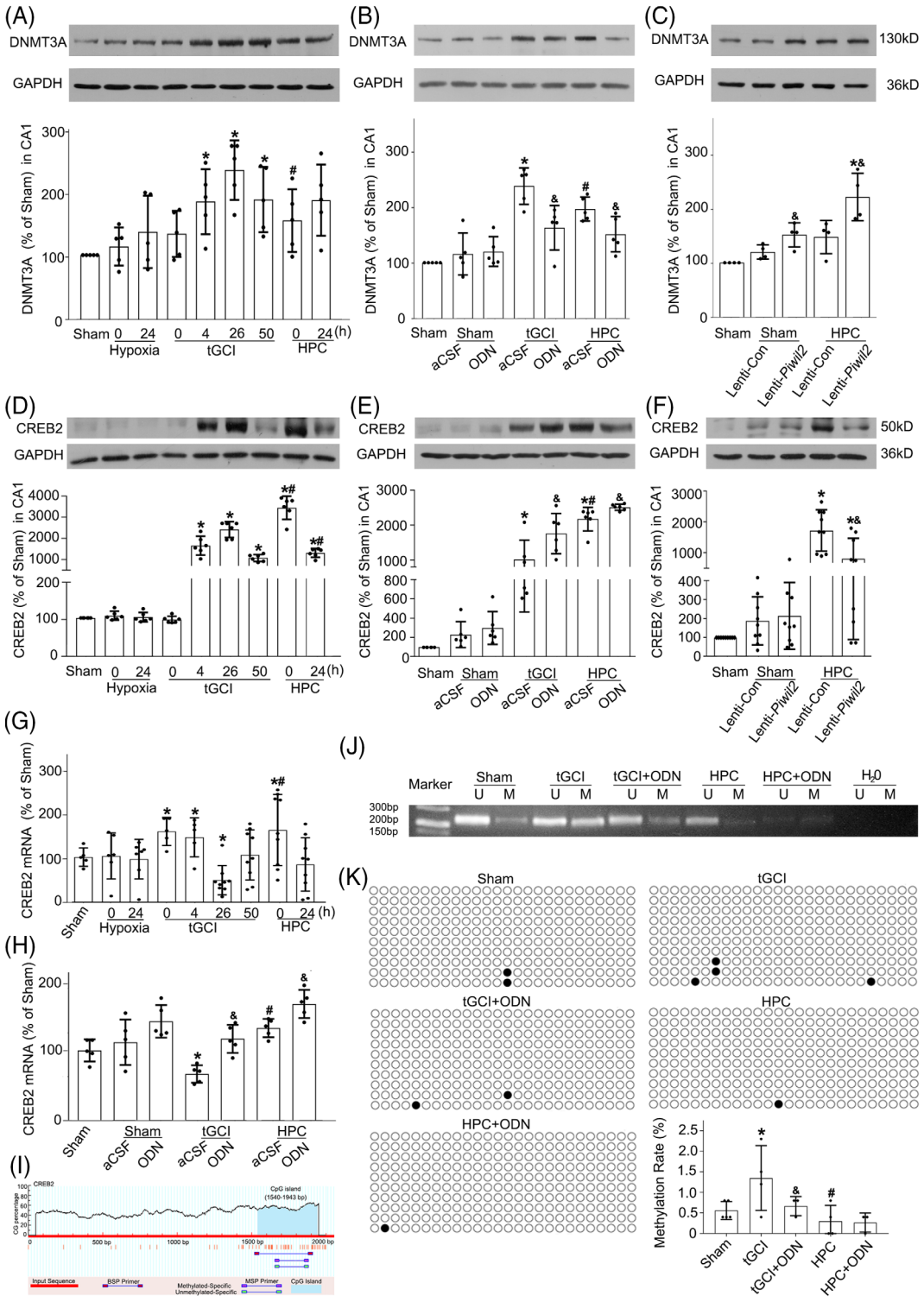

FIGURE 5 Legend on next page.

To determine whether HPC not only protects against the injury on the dendritic structure of hippocampal neurons but also improves cognition after tGCI, Morris water maze was used to assess the cognitive function of rats (Figure 6F–J). After 5 d of training, all groups of rats improved their ability to locate the platform. However, the path length and escape latency in tGCI rats were longer than that of Sham. Notably, compared with tGCI group, HPC significantly shortened the path length from the 1st to 5th day of training and escape latency on the 3rd and 5th day of training. To rule out the possibilities that the spatial memory deficits in tGCI rats were caused

by the difference in swimming ability, swimming speed was recorded. However, no difference in the mean swimming velocity was observed among all the observed groups. Moreover, in the probe phase, retention of long-term spatial memory was analyzed. The results showed that the rats in the tGCI group spent shorter time in the target quadrant occupancy than that of Sham rats. It is worth noting that with HPC treatment the rats spent longer time in the target quadrant occupancy when compared to the rats in tGCI group. Further, we observed the effect of Piwil2 on the function of hippocampus caused by tGCI. As shown in Figure 6H–J, the knockdown of Piwil2 with AS-ODN in tGCI and HPC rats improved spatial learning and long-term memory, with shorter swimming path length and escape latency, and longer time in the target quadrant occupancy.

4 | DISCUSSION

In the present study, we delineated a novel role for Piwil2 in regulating CREB2 expression via epigenetic mechanism and mediating neuroprotection of HPC after tGCI in rats (Figure 7). Our data show that HPC downregulated the expression of Piwil2 in CA1 after tGCI, and reduced the level of de novo DNA methyltransferases, DNMT3A, which, in turn, abolished the tGCI-induced increase in methylation at the promoter of *CREB2*, and thus increasing the expression of CREB2 at both mRNA and protein levels. In addition, the reduction of Piwil2 induced by HPC restored dendrite complexity and dendrite length, and prevented the loss of dentritic spines in CA1 neurons, which consequently improved the learning and memory function of rats after tGCI.

Despite previous reports of piRNA expression in the mammalian brain, including piRNA dysregulation in response to pathological events, few studies focused on the functional role of Piwi-like proteins or the Piwi pathway as a whole. Zhao et al. [42] reported that *Piwil1* regulates the polarity and migration of neurons in developing mouse neocortex. Another study demonstrated that the deletion of *Piwil2* in mice would bring about its behavioral deficits [18]. Interestingly, in this study, we demonstrated that HPC attenuated tGCI-induced elevation of Piwil2 at both the mRNA and protein levels in CA1. Several studies indicated that Piwil2 directly or indirectly regulate signaling pathways or the activity of pro-survival factors to protect the tumor cells from death [16, 17, 43]. For example, a study in the cells of lung cancer found that silencing Piwil2 expression arrests cells at G2/M phase of cell cycle and induces apoptotic cell death [43]. In addition, it has been shown that Piwil2 represses the tumor suppressor p53 [17] and upregulates anti-apoptotoc factor Bcl-xL [44], leading to the proliferation and survival of tumor cells. However, the role of Piwil2 in regulating cell survival in nonmalignant cells remains unknown. One study reported that silencing Piwil2 and Piwil4 decreased caspase-3 and caspase-7 activity and attenuated unfolded protein response (UPR)-related cell death in human airway epithelial cells [45]. Similarly, in our study, silencing Piwil2 in CA1 effectively ameliorated post-ischemic neuronal death and decreased the expression of the key apoptotic proteases, such as cleaved caspase-3 and caspase-9. As expected, the overexpression of Piwil2 in CA1 with Piwil2-carried lentivirus abolished HPC-induced neuroprotection. This study firstly revealed the involvement of Piwil2 in neuronal damage after cerebral ischemia in rats.

The expression of piRNAs has been detected in the mammalian brain [18, 36, 46, 47]. In rodent brain, the expression of many piRNAs (>100) are highly altered during focal ischemic condition, and about 25 of them are identified as a stroke responsive piRNAs using bioinformatics analysis [47]. Consistently, in our study, we identified a cohort of piRNAs in CA1 of rats. Furthermore, we demonstrated directly contrast changes of Piwil2-interacting piRNAs in CA1 after tGCI, as compared to those in HPC rats. Therefore, this study revealed that PIWI/piRNAs respond to ischemic brain damage and neuroprotection mediated by HPC. To the best of

FIGURE 5 HPC reduces the expression of DNMT3A, inhibits the DNA methylation of *CREB2* and increases the expression of CREB2 in CA1. (A) Western blot analysis of DNMT3A expression in CA1. (B) Representative images of Western blot show the expression of DNMT3A in CA1 after tGCI with and without Piwil2 AS-ODN administration. (C) Representative immunoblots of DNMT3A expression in CA1 after HPC with and without *Piwil2* lentiviral vectors administration. (D) Representative immunoblots of CREB2 expression in CA1. (E) Representative images of Western blot show the expression of CREB2 in CA1 after tGCI with and without Piwil2 AS-ODN administration. (F) Representative immunoblots of CREB2 expression in CA1 after HPC with and without *Piwil2* lentiviral vectors administration. (G) RT-qPCR analysis of CREB2 mRNA in CA1. (H) RT-qPCR analysis of CREB2 mRNA in CA1 after tGCI with and without Piwil2 AS-ODN administration. Data are expressed as percentage of value of Sham animals. Each bar represents the mean ± SD. $^{*}p < 0.05$ vs. Sham animals (A–H), $^{\#}p < 0.05$ vs. tGCI groups at the same time point (A,D,G). $^{\#}P < 0.05$ vs. tGCI group and $^{\&}p < 0.05$ vs. tGCI group or HPC group administrated with aCSF (B,E,H), and $^{\&}p < 0.05$ vs. Sham or HPC group with injection of Lenti-Con (C,F). (I) Methylation status of CpG sites in the *CREB2* promoter region (from +1540 bp to +1943 bp) determined using MSP and BSP analysis. (J) The methylation status of *CREB2* gene was analyzed by MSP using two different sets of primers. U, unmethylated PCR products; M, methylated PCR products. PCR products are about 200 bp. (K) Quantification of the frequency of methylation at each CpG site of *CREB2* promoter. Data are expressed as percentage of total CpG methylation sites between +1540 bp to +1943 bp of the *CREB2* promoter. Each bar represents the mean ± SD. $^{*}p < 0.05$ vs. Sham animals, $^{\#}p < 0.05$ vs. tGCI group and $^{\&}p < 0.05$ vs. tGCI group or HPC group. Black dot, methylated; white dot, unmethylated. AS-ODN, antisense oligodeoxynucleotide; CREB2, cyclic AMP response element-binding 2; DNMT3A, DNA methyltransferase 3A; HPC, hypoxic postconditioning; Lenti-Con, Lenti-Control: scrambled lentivirus vector; lenti-*Piwil2*, *Piwil2*-carried lentivirus; Sham, sham-operated; tGCI, transient global cerebral ischemia

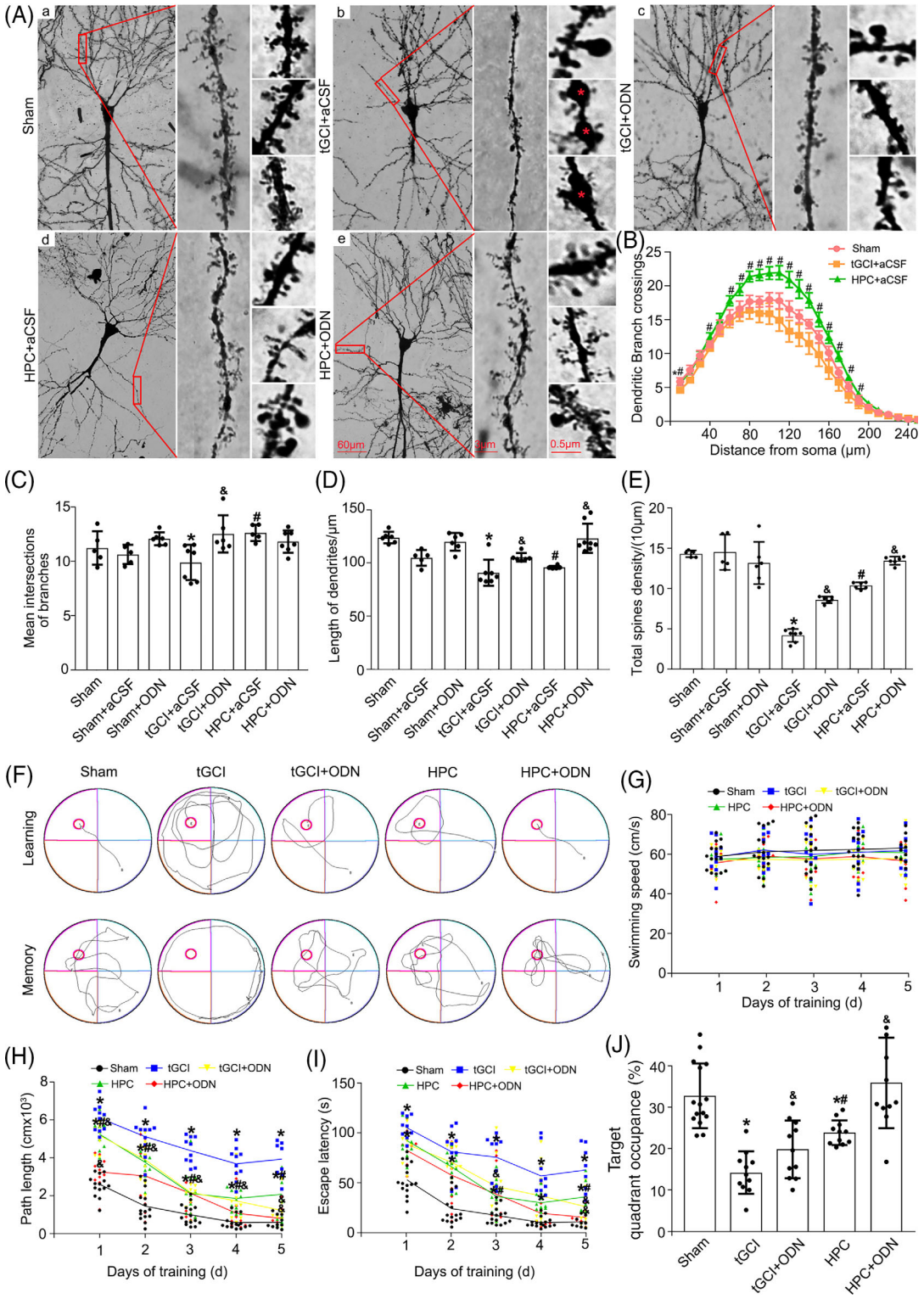

FIGURE 6 HPC enhances the plasticity of hippocampal dendritic spines and improves memory function after tGCI. (A) Representative reconstructions of CA1 pyramidal neurons using Golgi staining. Magnified views of the red-boxed regions on middle column are z-stack images of dendrites. Magnified views on the right show structural changes in dendritic spines during tGCI or HPC with and without Piwil2 AS-ODN administration. Asterisk indicates a spine partially collapsed down into the dendritic shaft during tGCI. (B,C) Sholl analyses of dendrites in CA1 pyramidal neurons. (D,E) Quantification of neuronal morphometric analyses, length of dendritic branch and density of dendrite spines. Cognitive function was tested by Morris water maze. (F) Representative path tracings in each quadrant during the training period (learning) and the probe trial (memory). The swimming speed (G), path length (H) and escape latency (I) were recorded during the training period. (J) The percentage of time spent in the target quadrant to total time (30 s) was recorded at day 7 after tGCI. Data are expressed as the mean ± SD. $^{*}p < 0.05$ vs. sham animals, $^{\#}p < 0.05$ vs. tGCI group, and $^{\&}p < 0.05$ vs. tGCI or HPC group. aCSF, artificial cerebrospinal fluid; AS-ODN, antisense oligodeoxynucleotide; HPC, hypoxic postconditioning; Sham, sham-operated; tGCI, transient global cerebral ischemia

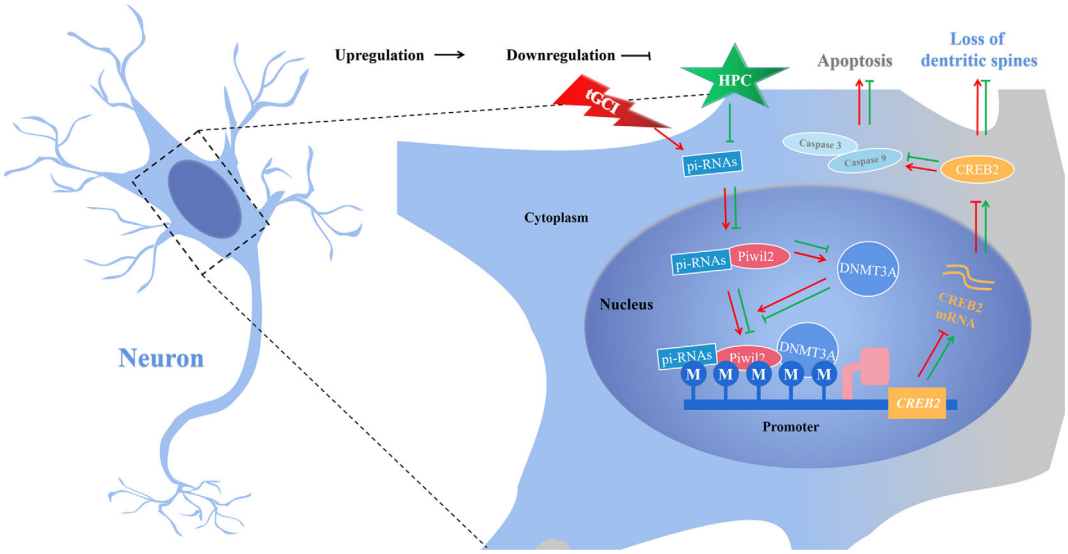

FIGURE 7 Schematic depicting mechanism by which HPC protects neurons against tGCI in CA1 through Piwil2-mediated epigenetics. HPC downregulates the expression of Piwil2 in CA1 after tGCI, and reduces the level of de novo DNA methyltransferases, DNMT3A, which, in turn, abolishes the tGCI-induced increase in methylation at the promoter of *CREB2*, and thus increasing the expression of CREB2 at both mRNA and protein levels. In addition, the reduction of Piwil2 induced by HPC restores dendrite complexity and dendrite length, and prevents the loss of dentritic spines in CA1 neurons, which consequently improves the learning and memory function of rats after tGCI. CREB2, cyclic AMP response element-binding 2; DNMT3A, DNA methyltransferase 3A; HPC, hypoxic postconditioning; tGCI, transient global cerebral ischemia

our knowledge, this is the first study ever on piRNAs associated with Piwil2 in cerebral ischemic tolerance.

Piwil2/piRNAs complex can exhibit multifunctional role depending on their location and binding partners. The distribution of PIWI/piRNAs complex in different subcellular locations such as cytoplasm, mitochondria, and nucleus suggests diversified PIWI functions in somatic cells. For instance, the nuclear PIWI/piRNAs regulate gene expression and transposons by epigenetic modifications, whereas the cytoplasmic PIWI proteins, mostly independent on its partner piRNAs, modulate cellular signaling by directly regulating the post-translational modification [9]. Contrary to the cytoplasmic localization of Piwil2 in mouse hippocampal neurons [36], we observed a predominant nucleic localization of Piwil2 in rat hippocampal neurons, similar to what was observed by Rajasethupathy et al., in *Aplysia* sensory neurons [10]. These results suggest a nuclear function for Piwil2/piRNAs complex, such as DNA methylation. It is generally known that DNA methylation occurs on CpG islands, the regions that are enriched with CG dinucleotides and are usually located at the promoter regions of genes, where cytosine at the 5′ end of CpG is converted into 5′ methyl-cytosine by DNMTs. Therefore, to further support the nuclear function for Piwil2/piRNAs complex, we measured DNMTs and the DNA methylation level of target gene. Mammalian system consists of three active DNMTs, DNMT1, DNMT3A, and DNMT3B. It is evident that PIWI/piRNAs can regulate the expression and activity of DNMTs [48–50]. Interestingly, in our present study of Piwil2-interacting piRNAs, the results from the targets prediction of the GO term and KEGG pathway annotations showed that DNMT3A may be a potential common target of 7 piRNAs that presented a relatively high difference in expression between tGCI and HPC groups. As expected, HPC attenuated tGCI-induced elevation of DNMT3A in CA1. Furthermore, the knockdown of Piwil2 decreased DNMT3A expression in CA1 after tGCI, whereas the overexpression of Piwil2 elevated its expression after HPC. Collectively, these data suggest that Piwil2/piRNAs may be direct regulators of the DNMT3A expression in CA1 of rats after cerebral ischemia.

A growing number of studies supports that PIWI/piRNAs pathway not only represses transposons, but also regulates protein-coding genes. For example, two studies demonstrate that PIWI/piRNAs pathway represses the expression of a gene by the methylation of its promoter [10, 51]. Notably, in the present work, several proteins scored high as possible targets for three differentially expressed piRNAs in CA1 between tGCI and HPC groups. Among these, CREB2 is the common target. To date, studies have demonstrated diverse roles for CREB2 in the brain. In response to pathological stress, CREB2 has been described as either promoting or suppressing neuron dysfunction or death [52–54]. In our study, we observed that the level of CREB2 protein increased in CA1 of rats with tGCI, but began to decrease at 50 h after reperfusion. However, the rats treated with HPC maintained the high expression level of CREB2 in CA1 after tGCI. These results indicate that HPC may prevent neuronal death by increasing CREB2 level in CA1 after tGCI-induced injury. It is evident that CREB2 exerts antioxidative effects on cancer cells [55, 56]. In addition, our prior work has shown that HPC reduces

neuronal death in CA1 after tGCI via its antioxidative roles [57]. Therefore, the present study confers the evidence that HPC prevents the downregulation of CREB2 and inhibits oxidative stress, thereby contributing to anti-apoptosis. More importantly, a major focal point in our study is the mechanism by which PIWI/piRNA pathway regulates the expression of CREB2. Much of the effort in understanding CREB2 regulation has focused on its translational control by eukaryotic translation initiation factor 2α. Notably, the discovery in the present study that the inhibition of Piwil2 in CA1 abolished the tGCI-induced increase in methylation at the promoter of *CREB2*, which in turn resulted in an increase in the expression of CREB2 at both mRNA and protein levels, suggesting that the Piwil2/piRNAs regulates the expression of CREB2 via the CREB2 promoter by DNA methylation. This result serves as the first evidence that Piwil2 exerts its epigenetic functions by modulating the DNA methylations within CpG island of *CREB2* promoters and contributes to the neuronal damage after cerebral ischemia.

CREB2 has already been reported as an essential modulator of synaptic plasticity and memory [27, 28]. Moreover, given that the differentially expressed piRNAs in CA1 were mainly clustered for axon guidance and synaptic functions, we therefore focused on the changes in dendritic spine morphology and hippocampal-dependent behavior. Here our study showed that tGCI leads to the loss of dendritic spines and the reduction in dendrite complexity and length of CA1 neurons in the dorsal hippocampus, accompanied by the impairment of memory. This process was readily reversed by HPC or Piwil2 silencing after tGCI. How CREB2 regulates synaptic function after cerebral ischemia has not been reported. A prior study showed that CREB2 knockdown reduced the density of dendritic postsynaptic density-95 (PSD-95) and glutamate receptor 1 (GluR1) puncta in cultures of hippocampal neurons, which in turn reduced the density of dendritic mushroom spines [27]. Future studies should address the issues that whether the reduction of CREB2 after tGCI reduces the expression of PSD-95 and/or GluR1 in CA1.

The results from this study, however, have yet to be tested in aged group of animals. It is known that aging and comorbidities have a major impact on the incidence, consequences and the efficacy of any therapy. Age is the single and principal nonmodifiable risk factor for ischemic stroke. Compared with the young brain, the aged displays more vulnerable to ischemia, and aged patients with stroke have higher mortality and morbidity and poorer functional outcomes than the young counterparts [58, 59]. Similarly, comorbidities, such as hypertension, diabetes, obesity and hyperlipidemia, not only contribute to the increased incidence of ischemic stroke as risk factors, but also accelerate the progression of brain damage after cerebral ischemia [60, 61]. They would have impacts on the efficacy of their therapy. Therefore, in order to elucidate the roles and the underlying molecular mechanisms of Piwil2/piRNAs pathway in cerebral ischemic tolerance induced by HPC, an preclinical model of ischemic stroke which could accurately mimic human stroke by incorporating aged and reproductively senescent rodents, as well as animals with comorbid conditions should be established.

In summary, our findings establish the roles for Piwil2/piRNAs in the epigentic regulation of the expression of CREB2 and the neuroprotection of HPC against tGCI in rats. The downregulation of Piwil2 in CA1 of rats induced by HPC inhibited the hypermethylation of CREB2 and promoted its transcription by retraining DNMT3A induced CpG methylation in promoter site, and consequently led to an increase of CREB2 after tGCI. The present findings significantly extended the epigenetic regulatory role of Piwil2/piRNAs pathway to neuron. We also provided insights on the effects of Piwil2/piRNAs on neuronal plasticity in rats. Further studies should address whether altered Piwil2-interacting piRNAs might contribute to *CREB2* gene regulation and thereby mediate neuroprotection against tGCI in rats. Answering these important questions will enable us to develop innovative Piwil2/piRNAs-based therapies for ischemic stroke.

AUTHOR CONTRIBUTIONS

En Xu and Lixuan Zhan conceived the study and experiments, designed and assembled all figures. Meiyan Chen, Taoyan Pang, Xinyu Li, Long Long, and Linhui Peng performed the experiments with help of Weiwen Sun and Donghai Liang. Lixuan Zhan, Meiyan Chen, Taoyan Pang, and Xinyu Li performed data analysis. En Xu and Lixuan Zhan wrote the manuscript. All authors read and approved the final manuscript.

ACKNOWLEDGMENTS

We thank Cloud-Seq Biotech Ltd. Co. (Shanghai, China) for the piRNA-seq service and the subsequent bioinformatics analysis. Our sincere thanks go to Peifeng Du (Guangzhou International Bio Island Co., Ltd) for editing this paper. This work is supported by the National Natural Science Foundation of China (No. 81873745, 81971124), and the Science and Technology Program of Guangzhou, China (No. 202002030072).

CONFLICT OF INTEREST

The authors declare that they have no competing interests.

DATA AVAILABILITY STATEMENT

The authors declare that all data supporting the results in this study are available within the paper and its Supplementary Information. Raw data are available from the corresponding author upon reasonable request. The small RNA-Seq data have been deposited in the GEO database, under accession number GSE163298

and GSE163299. Source data are provided with this paper.

ETHICS STATEMENT

The animal experiments were conducted according to the *Animal Research*: *Reporting In Vivo Experiments (ARRIVE)* guidelines. The study was approved by the Animals Care and Use Committee of Guangzhou Medical University (Guangzhou, China).

ORCID

En Xu https://orcid.org/0000-0003-4874-6373

REFERENCES

1. Katan M, Luft A. Global burden of stroke. Semin Neurol. 2018; 38:208–11. https://doi.org/10.1055/s-0038-1649503
2. Chen Z, Jiang B, Ru X, Sun H, Sun D, Liu X, et al. Mortality of stroke and its subtypes in China: results from a nationwide population-based survey. Neuroepidemiology. 2017;48:95–102. https://doi.org/10.1159/000477494
3. Dharap A, Nakka VP, Vemuganti R. Effect of focal ischemia on long noncoding RNAs. Stroke. 2012;43:2800–2. https://doi.org/10.1161/STROKEAHA.112.669465
4. Schweizer S, Meisel A, Märschenz S. Epigenetic mechanisms in cerebral ischemia. J Cereb Blood Flow Metab. 2013;33:1335–46. https://doi.org/10.1038/jcbfm.2013.93
5. Shen Y, Peng C, Bai Q, Ding Y, Yi X, Du H, et al. Epigenome-wide association study indicates hypomethylation of MTRNR2L8 in large-artery atherosclerosis stroke. Stroke. 2019;50:1330–8. https://doi.org/10.1161/STROKEAHA.118.023436
6. Zhou S, Zhang Y, Wang L, Zhang Z, Cai B, Liu K, et al. CDKN2B methylation is associated with carotid artery calcification in ischemic stroke patients. J Transl Med. 2016;14:333. https://doi.org/10.1186/s12967-016-1093-4
7. Deng GX, Xu N, Huang Q, Tan JY, Zhang Z, Li XF, et al. Association between promoter DNA methylation and gene expression in the pathogenesis of ischemic stroke. Aging (Albany NY). 2019; 11:7663–77. https://doi.org/10.18632/aging.102278
8. Luteijn MJ, Ketting RF. PIWI-interacting RNAs: from generation to transgenerational epigenetics. Nat Rev Genet. 2013;14:523–34. https://doi.org/10.1038/nrg3495
9. Ponnusamy M, Yan KW, Liu CY, Li PF, Wang K. PIWI family emerging as a decisive factor of cell fate: an overview. Eur J Cell Biol. 2017;96:746–57. https://doi.org/10.1016/j.ejcb.2017.09.004
10. Rajasethupathy P, Antonov I, Sheridan R, Frey S, Sander C, Tuschl T, et al. A role for neuronal piRNAs in the epigenetic control of memory-related synaptic plasticity. Cell. 2012;149:693–707. https://doi.org/10.1016/j.cell.2012.02.057
11. Perrat PN, DasGupta S, Wang J, Theurkauf W, Weng Z, Rosbash M, et al. Transposition-driven genomic heterogeneity in the *Drosophila* brain. Science. 2013;340:91–5. https://doi.org/10.1126/science.1231965
12. Kim KW, Tang NH, Andrusiak MG, Wu Z, Chisholm AD, Jin Y. A neuronal piRNA pathway inhibits axon regeneration in *C. elegans*. Neuron. 2018;97:511–519.e6. https://doi.org/10.1016/j.neuron.2018.01.014
13. Phay M, Kim HH, Yoo S. Analysis of piRNA-like small noncoding RNAs present in axons of adult sensory neurons. Mol Neurobiol. 2018;55:483–94. https://doi.org/10.1007/s12035-016-0340-2
14. Leighton LJ, Wei W, Marshall PR, Ratnu VS, Li X, Zajaczkowski EL, et al. Disrupting the hippocampal Piwi pathway enhances contextual fear memory in mice. Neurobiol Learn Mem. 2019;161:202–9. https://doi.org/10.1016/j.nlm.2019.04.002
15. Sasaki T, Shiohama A, Minoshima S, Shimizu N. Identification of eight members of the Argonaute family in the human genome. Genomics. 2003;82:323–30. https://doi.org/10.1016/s0888-7543(03)00129-0
16. Lee JH, Schutte D, Wulf G, Fuzesi L, Radzun HJ, Schweyer S, et al. Stem-cell protein Piwil2 is widely expressed in tumors and inhibits apoptosis through activation of Stat3/Bcl-XL pathway. Hum Mol Genet. 2006;15:201–11. https://doi.org/10.1093/hmg/ddi430
17. Lu Y, Zhang K, Li C, Yao Y, Tao D, Liu Y, et al. Piwil2 suppresses p53 by inducing phosphorylation of signal transducer and activator of transcription 3 in tumor cells. PLoS ONE. 2012;7:e30999. https://doi.org/10.1371/journal.pone.0030999
18. Nandi S, Chandramohan D, Fioriti L, Melnick AM, Hébert JM, Mason CE, et al. Roles for small noncoding RNAs in silencing of retrotransposons in the mammalian brain. Proc Natl Acad Sci U S A. 2016;113:12697–702. https://doi.org/10.1073/pnas.1609287113
19. Aravin AA, Sachidanandam R, Bourc'his D, Schaefer C, Pezic D, Toth KF, et al. A piRNA pathway primed by individual transposons is linked to de novo DNA methylation in mice. Mol Cell. 2008;31:785–99. https://doi.org/10.1016/j.molcel.2008.09.003
20. Aravin AA, Sachidanandam R, Girard A, Fejes-Toth K, Hannon GJ. Developmentally regulated piRNA clusters implicate MILI in transposon control. Science. 2007;316:744–7. https://doi.org/10.1126/science.1142612
21. Kuramochi-Miyagawa S, Watanabe T, Gotoh K, Totoki Y, Toyoda A, Ikawa M, et al. DNA methylation of retrotransposon genes is regulated by Piwi family members MILI and MIWI2 in murine fetal testes. Genes Dev. 2008;22:908–17. https://doi.org/10.1101/gad.1640708
22. Ameri K, Harris AL. Activating transcription factor 4. Int J Biochem Cell Biol. 2008;40:14–21. https://doi.org/10.1016/j.biocel.2007.01.020
23. Whitney ML, Jefferson LS, Kimball SR. ATF4 is necessary and sufficient for ER stress-induced upregulation of REDD1 expression. Biochem Biophys Res Commun. 2009;379:451–5. https://doi.org/10.1016/j.bbrc.2008.12.079
24. Ye J, Koumenis C. ATF4, an ER stress and hypoxia-inducible transcription factor and its potential role in hypoxia tolerance and tumorigenesis. Curr Mol Med. 2009;9:411–6. https://doi.org/10.2174/156652409788167096
25. Li Y, Zhang Y, Fu H, Huang H, Lu Q, Qin H, et al. Hes1 knockdown exacerbates ischemic stroke following tMCAO by increasing ER stress-dependent apoptosis via the PERK/eIF2α/ATF4/CHOP signaling pathway. Neurosci Bull. 2020;36:134–42. https://doi.org/10.1007/s12264-019-00411-7
26. He Q, Li Z, Meng C, Wu J, Zhao Y, Zhao J. Parkin-dependent mitophagy is required for the inhibition of ATF4 on NLRP3 inflammasome activation in cerebral ischemia-reperfusion injury in rats. Cell. 2019;8:897. https://doi.org/10.3390/cells8080897
27. Liu J, Pasini S, Shelanski ML, Greene LA. Activating transcription factor 4 (ATF4) modulates post-synaptic development and dendritic spine morphology. Front Cell Neurosci. 2014;8:177. https://doi.org/10.3389/fncel.2014.00177
28. Pasini S, Corona C, Liu J, Greene LA, Shelanski ML. Specific downregulation of hippocampal ATF4 reveals a necessary role in synaptic plasticity and memory. Cell Rep. 2015;11:183–91. https://doi.org/10.1016/j.celrep.2015.03.025
29. Wortel I, van der Meer LT, Kilberg MS, van Leeuwen FN. Surviving stress: modulation of ATF4-mediated stress responses in normal and malignant cells. Trends Endocrinol Metab. 2017;28:94–806. https://doi.org/10.1016/j.tem.2017.07.003
30. Mann IK, Chatterjee R, Zhao J, He X, Weirauch MT, Hughes TR, et al. CG methylated microarrays identify a novel methylated sequence bound by the CEBPB|ATF4 heterodimer

that is active in vivo. Genome Res. 2013;23:988–97. https://doi.org/10.1101/gr.146654.112
31. Nitatori T, Sato N, Waguri S, Karasawa Y, Araki H, Shibanai K, et al. Delayed neuronal death in the CA1 pyramidal cell layer of the gerbil hippocampus following transient ischemia is apoptosis. J Neurosci. 1995;15:1001–11. https://doi.org/10.1523/JNEUROSCI.15-02-01001.1995
32. Kasai H, Matsuzaki M, Noguchi J, Yasumatsu N, Nakahara H. Structure-stability-function relationships of dendritic spines. Trends Neurosci. 2003;26:360–8. https://doi.org/10.1016/S0166-2236(03)00162-0
33. Murphy TH, Li P, Betts K, Liu R. Two-photon imaging of stroke onset in vivo reveals that NMDA-receptor independent ischemic depolarization is the major cause of rapid reversible damage to dendrites and spines. J Neurosci. 2008;28:756–1772. https://doi.org/10.1523/JNEUROSCI.5128-07.2008
34. Zhang S, Boyd J, Delaney K, Murphy T. Rapid reversible changes in dendritic spine structure in vivo gated by the degree of ischemia. J Neurosci. 2005;25:5333–8. https://doi.org/10.1523/JNEUROSCI.1085-05.2005
35. Zhan L, Li D, Liang D, Wu B, Zhu P, Wang Y, et al. Activation of Akt/FoxO and inactivation of MEK/ERK pathways contribute to induction of neuroprotection against transient global cerebral ischemia by delayed hypoxic postconditioning in adult rats. Neuropharmacology. 2012;63:873–82. https://doi.org/10.1016/j.neuropharm.2012.06.035
36. Lee EJ, Banerjee S, Zhou H, Jammalamadaka A, Arcila M, Manjunath BS, et al. Identification of piRNAs in the central nervous system. RNA. 2011;17:1090–9. https://doi.org/10.1261/rna.2565011
37. Pulsinelli WA, Brierley JB. A new model of bilateral hemispheric ischemia in the unanesthetized rat. Stroke. 1979;10:267–72. https://doi.org/10.1161/01.str.10.3.267
38. Zhan L, Liu L, Li K, Wu B, Liu D, Liang D, et al. Neuroprotection of hypoxic postconditioning against global cerebral ischemia through influencing posttranslational regulations of heat shock protein 27 in adult rats. Brain Pathol. 2017;27:822–38. https://doi.org/10.1111/bpa.12472
39. Zhan L, Wang T, Li W, Xu ZC, Sun W, Xu E. Activation of Akt/-FoxO signaling pathway contributes to induction of neuroprotection against transient global cerebral ischemia by hypoxic preconditioning in adult rats. J Neurochem. 2010;114:897–908. https://doi.org/10.1111/j.1471-4159.2010.06816.x
40. Juárez I, Gratton A, Flores G. Ontogeny of altered dendritic morphology in the rat prefrontal cortex, hippocampus, and nucleus accumbens following Cesarean delivery and birth anoxia. J Comp Neurol. 2008;507:1734–47. https://doi.org/10.1002/cne.21651
41. Rubinow MJ, Drogos LL, Juraska JM. Age-related dendritic hypertrophy and sexual dimorphism in rat basolateral amygdala. Neurobiol Aging. 2009;30:137–46. https://doi.org/10.1016/j.neurobiolaging.2007.05.006
42. Zhao PP, Yao MJ, Chang SY, Gou LT, Liu MF, Qiu ZL, et al. Novel function of PIWIL1 in neuronal polarization and migration via regulation of microtubule-associated proteins. Mol Brain. 2015;8:39. https://doi.org/10.1186/s13041-015-0131-0
43. Qu X, Liu J, Zhong X, Li X, Zhang Q. PIWIL2 promotes progression of non-small cell lung cancer by inducing CDK2 and cyclin a expression. J Transl Med. 2015;13:301. https://doi.org/10.1186/s12967-015-0666-y
44. Lee JH, Jung C, Javadian-Elyaderani P, Schweyer S, Schütte D, Shoukier M, et al. Pathways of proliferation and antiapoptosis driven in breast cancer stem cells by stem cell protein piwil2. Cancer Res. 2010;70:4569–79. https://doi.org/10.1158/0008-5472.CAN-09-2670
45. Gebert M, Bartoszewska S, Janaszak-Jasiecka A, Moszyńska A, Cabaj A, Króliczewski J, et al. PIWI proteins contribute to apoptosis during the UPR in human airway epithelial cells. Sci Rep. 2018;8:16431. https://doi.org/10.1038/s41598-018-34861-2
46. Qiu W, Guo X, Lin X, Yang Q, Zhang W, Zhang Y, et al. Transcriptome-wide piRNA profiling in human brains of Alzheimer's disease. Neurobiol Aging. 2017;57:170–7. https://doi.org/10.1016/j.neurobiolaging.2017.05.020
47. Dharap A, Nakka VP, Vemuganti R. Altered expression of PIWI RNA in the rat brain after transient focal ischemia. Stroke. 2011;42:1105–9. https://doi.org/10.1161/STROKEAHA.110.598391
48. Chen KM, Campbell E, Pandey RR, Yang Z, McCarthy AA, Pillai RS. Metazoan maelstrom is an RNA-binding protein that has evolved from an ancient nuclease active in protists. RNA. 2015;21:833–9. https://doi.org/10.1261/rna.049437.114
49. Siddiqi S, Matushansky I. Piwis and piwi-interacting RNAs in the epigenetics of cancer. J Cell Biochem. 2012;113:373–80. https://doi.org/10.1002/jcb.23363
50. Yan H, Wu QL, Sun CY, Ai LS, Deng J, Zhang L, et al. piRNA-823 contributes to tumorigenesis by regulating de novo DNA methylation and angiogenesis in multiple myeloma. Leukemia. 2015;29:196–206. https://doi.org/10.1038/leu.2014.135
51. Watanabe T, Tomizawa S, Mitsuya K, Totoki Y, Yamamoto Y, Kuramochi-Miyagawa S, et al. Role for piRNAs and noncoding RNA in de novo DNA methylation of the imprinted mouse Rasgrf1 locus. Science. 2011;332:848–52. https://doi.org/10.1126/science.1203919
52. Sun X, Liu J, Crary JF, Malagelada C, Sulzer D, Greene LA, et al. ATF4 protects against neuronal death in cellular Parkinson's disease models by maintaining levels of parkin. J Neurosci. 2013;33:2398–407. https://doi.org/10.1523/JNEUROSCI.2292-12.2013
53. Baleriola J, Walker CA, Jean YY, Crary JF, Troy CM, Nagy PL, et al. Axonally synthesized ATF4 transmits a neurodegenerative signal across brain regions. Cell. 2014;158:1159–72. https://doi.org/10.1016/j.cell.2014.07.001
54. Rittiner JE, Caffall ZF, Hernández-Martinez R, Sanderson SM, Pearson JL, Tsukayama KK, et al. Functional genomic analyses of Mendelian and sporadic disease identify impaired eIF2α signaling as a generalizable mechanism for dystonia. Neuron. 2016;92:1238–51. https://doi.org/10.1016/j.neuron.2016.11.012
55. Hocsak E, Szabo V, Kalman N, Antus C, Cseh A, Sumegi K, et al. PARP inhibition protects mitochondria and reduces ROS production via PARP-1-ATF4-MKP-1-MAPK retrograde pathway. Free Radic Biol Med. 2017;108:770–84. https://doi.org/10.1016/j.freeradbiomed.2017.04.018
56. Wang SF, Wung CH, Chen MS, Chen CF, Yin PH, Yeh TS, et al. Activated integrated stress response induced by Salubrinal promotes cisplatin resistance in human gastric cancer cells via enhanced xCT expression and glutathione biosynthesis. Int J Mol Sci. 2018;19:3389. https://doi.org/10.3390/ijms19113389
57. Wen H, Liu L, Zhan L, Liang D, Li L, Liu D, et al. Neuroglobin mediates neuroprotection of hypoxic postconditioning against transient global cerebral ischemia in rats through preserving the activity of Na+/K+ ATPases. Cell Death Dis. 2018;9:635. https://doi.org/10.1038/s41419-018-0656-0
58. Joseph C, Buga AM, Vintilescu R, Balseanu AT, Moldovan M, Junker H, et al. Prolonged gaseous hypothermia prevents the upregulation of phagocytosis-specific protein annexin 1 and causes low-amplitude EEG activity in the aged rat brain after cerebral ischemia. J Cereb Blood Flow Metab. 2012;32:1632–42. https://doi.org/10.1038/jcbfm.2012.65
59. Popa-Wagner A, Buga AM, Doeppner TR, Hermann DM. Stem cell therapies in preclinical models of stroke associated with aging. Front Cell Neurosci. 2014;8:347. https://doi.org/10.3389/fncel.2014.00347
60. Popa-Wagner A, Dumitrascu DI, Capitanescu B, Petcu EB, Surugiu R, Fang WH, et al. Dietary habits, lifestyle factors and neurodegenerative diseases. Neural Regen Res. 2020;15:394–400. https://doi.org/10.4103/1673-5374.266045

61. Candelario-Jalil E, Paul S. Impact of aging and comorbidities on ischemic stroke outcomes in preclinical animal models: a translational perspective. Exp Neurol. 2021;335:113494. https://doi.org/10.1016/j.expneurol.2020.113494

SUPPORTING INFORMATION

Additional supporting information can be found online in the Supporting Information section at the end of this article.

How to cite this article: Zhan L, Chen M, Pang T, Li X, Long L, Liang D, et al. Attenuation of Piwil2 induced by hypoxic postconditioning prevents cerebral ischemic injury by inhibiting *CREB2* promoter methylation. Brain Pathology. 2023;33(1):e13109. https://doi.org/10.1111/bpa.13109